Parity-Dependent Moiré Superlattices in Graphene/*h*-BN Heterostructures: A Route to Mechanomutable Metamaterials

Wengen Ouyang,[1] Oded Hod,[2,*] and Michael Urbakh[2]

[1]*Department of Engineering Mechanics, School of Civil Engineering, Wuhan University, Wuhan, Hubei 430072, China*

[2]*Department of Physical Chemistry, School of Chemistry and The Sackler Center for Computational Molecular and Materials Science, The Raymond and Beverly Sackler Faculty of Exact Sciences, Tel Aviv University, Tel Aviv 6997801, Israel*

(Received 29 November 2020; accepted 29 April 2021; published 27 May 2021)

The superlattice of alternating graphene/*h*-BN few-layered heterostructures is found to exhibit strong dependence on the parity of the number of layers within the stack. Odd-parity systems show a unique flamingolike pattern, whereas their even-parity counterparts exhibit regular hexagonal or rectangular superlattices. When the alternating stack consists of 7 layers or more, the flamingo pattern becomes favorable, regardless of parity. Notably, the out-of-plane corrugation of the system strongly depends on the shape of the superstructure resulting in significant parity dependence of its mechanical properties. The predicted phenomenon originates in an intricate competition between moiré patterns developing at the interface of consecutive layers. This mechanism is of general nature and is expected to occur in other alternating stacks of closely matched rigid layered materials as demonstrated for homogeneous alternating junctions of twisted graphene and *h*-BN. Our findings thus allow for the rational design of mechanomutable metamaterials based on van der Waals heterostructures.

DOI: 10.1103/PhysRevLett.126.216101

Heterojunctions of vertically assembled van der Waals (vdW) layered materials [1] have attracted great scientific and technological interest since they exhibit diverse physical properties and carry great technological potential in various fields including electronics, optics, mechanics, and tribology [1–7]. Among the numerous possible vdW heterostructures graphene and hexagonal boron nitride (*h*-BN) junctions have attracted particular interest [8] as potential building blocks for field effect transistors [9,10], thermoelectric devices [11], solar cells, light-emitting diodes, and photodetectors [12–14].

The versatility of these systems stems from their unique electronic [15–19], magnetic [20,21], mechanical [22], and frictional properties [23–25], which are tightly intertwined with the moiré superlattices naturally occurring in such heterostructures [26,27]. By varying the twist angle between two adjacent layers, the moiré superlattices can be modified in a controlled manner opening a route to tune the corresponding material properties [15–19,28,29]. Further control can be gained via changing the number of stacked layers within the heterojunction. This has been demonstrated for *ABA*-stacked few-layer graphene, whose electronic properties exhibit dependence on the number of layers parity (being either odd or even) [30,31]. To the best of our knowledge, no similar parity effect has been observed in the mechanical properties of layered materials heterostructures, to date.

In the present Letter, we reveal a new phenomenon, where the symmetry of the moiré superlattice and the corresponding mechanical properties of vdW heterostructures depend on the parity of the number of layers. We demonstrate this for alternating few-layered graphene/*h*-BN stacks, where even layered structures present regular hexagonal or rectangular moiré patterns, whereas odd-layered structures exhibit a unique flamingolike pattern with relatively small Poisson's ratio. Furthermore, the sign of Poisson's ratio depends on the loading direction thus presenting novel auxetic metamaterial behavior [32–34]. Notably, above a stack thickness of seven layers, our calculations indicate that the flamingo pattern becomes preferential for both even- and odd-layered stacks.

Our model system consists of an aligned (nontwisted) stack of alternating layers of graphene and *h*-BN, whose number of layers is varied between 2 to 16. Intralayer interactions are modeled using the second-generation reactive empirical bond order potential [35] and the Tersoff potential [36], for graphene and *h*-BN, respectively. Interlayer interactions are modeled using our recently developed anisotropic interlayer potential [24,37–39]. To eliminate the edge effects, periodic boundary conditions (PBC) are applied in both the lateral directions and in the vertical dimension. To model finite thickness stacks, we choose a vacuum size of a 100 Å in the vertical dimension, which is sufficiently large to avoid interimage interactions that nullify above a cutoff value of 16 Å. We term this type of calculation 2D PBC, as it produces results which are identical to a purely lateral 2D PBC calculation. We use the term 3D PBC to describe simulations of bulk systems, where the periodicity in the vertical dimension is set to be the modeled supercell thickness plus one interlayer

distance. To assure convergence of the 3D PBC calculations with respect to the supercell thickness, we performed these calculations with two supercell models of 12 and 16 layers, both mimicking the same alternating bulk system. The comparison of the results obtained with these two bulk supercell thicknesses [see full symbols in Figs. 1(f) and 3] indicates that the PBC calculations are well converged. More details regarding the model system and the computational approach are provided in Secs. 1–3 of the Supplemental Material (SM) [40].

Because of the inherent intralayer lattice vectors mismatch of ~1.8% between graphene and *h*-BN layers, highly corrugated moiré patterns with flat nearly optimally stacked regions separated by narrow elevated ridges of suboptimal staking [22,37,48], appear following geometry optimization. In Fig. 1(a) the bilayer graphene/*h*-BN system is presented, showing the regular hexagonal moiré pattern with typical lateral dimensions of ~13.8 nm. Notably, when increasing the number of layers of the alternating stack, the competition between interlayer interactions at the different interfaces results in more involved moiré patterns [see Fig. 1(b)–1(e)]. The out-of-plane corrugation (peak-to-dip value) of these structures are summarized in Fig. 1(f). Surprisingly, strong parity dependence is observed up to a stack thickness of 7 layers, where the out-of-plane corrugation of the odd numbered heterostructures is 4–5 Å larger than that of the even numbered counterparts. Above this thickness, the parity dependence disappears and the lowest energy moiré pattern we could identify strongly deviates from the regular hexagonal superstructure obtained in the bilayer case (see Secs. 2.3–2.4 of the SM [40] for a discussion regarding this crossover behavior).

To understand the parity dependence of the deformation pattern, we plot in Fig. 2 the out-of-plane corrugation pattern for a consecutive series of alternating stacks of increasing thickness ranging from 2 to 9 layers. From this figure, the parity dependence is clearly evident, where the even stacks (up to 6 layers) present either the regular hexagonal structure or a related rectangular moiré structure, whereas the corresponding odd stacks exhibit a unique superstructure that resembles the shape of a flamingo (see Fig. 2). As mentioned above, for stack thickness exceeding

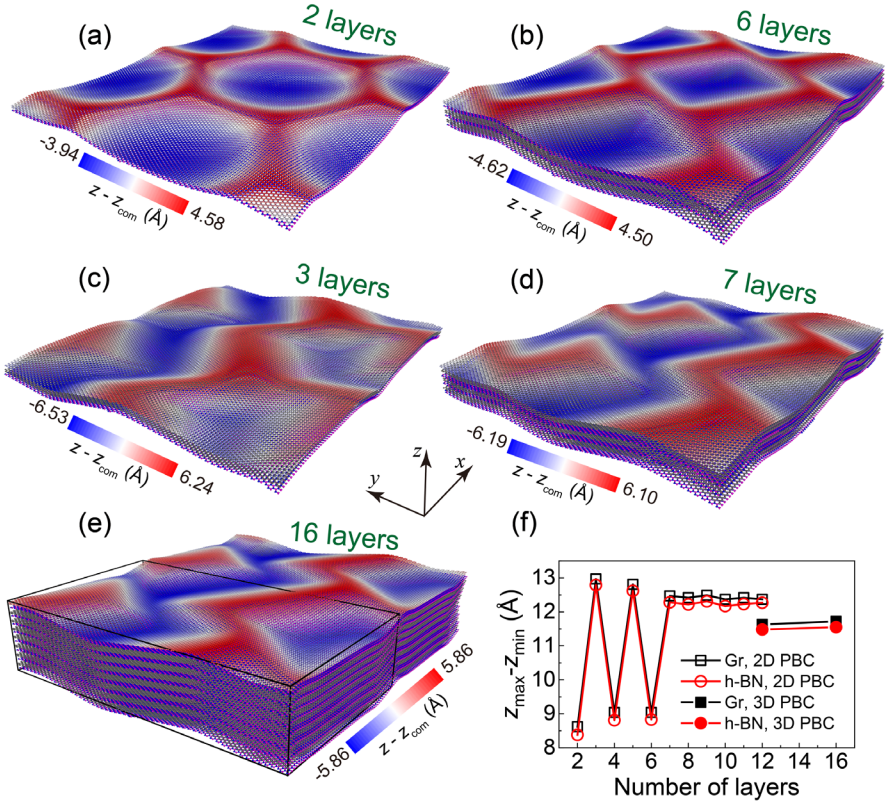

FIG. 1. Optimized alternating graphene/*h*-BN heterostructures of various number of layers obtained using two-dimensional (2D) periodic boundary conditions (PBC) in the lateral directions (a)–(d) and three-dimensional (3D) PBC (e). The atoms of the upper layers are colored according to their vertical height with respect to the center of mass of the layer (see corresponding color bars next to each panel). Mauve, blue, and gray spheres in the lower layers represent boron, nitrogen, and carbon atoms, respectively. For clarity, two unit cells are presented [see the black box in panel (e) for the actual supercell dimensions used in the simulations]. The out-of-plane corrugation (peak-to-dip value) in both graphene (black squares) and *h*-BN (red circles) layers as a function of the number of layers of the alternating graphene/*h*-BN heterostructures is presented in panel (f). Open symbols represent calculations obtained using 2D PBC and full symbols represent calculations performed using 3D PBC with different supercell thicknesses.

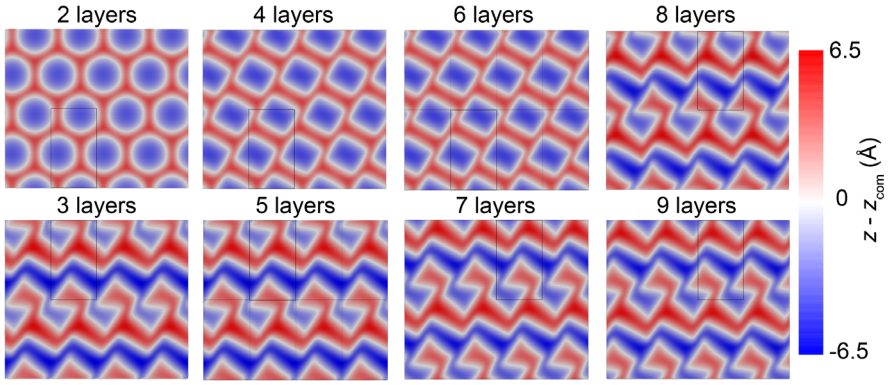

FIG. 2. Parity dependence of the out-of-plane distortion superstructures for alternating graphene/h-BN heterostructures. Top views of consecutive stacks of increasing thickness ranging from 2 to 9 layers are presented. The flamingo-shaped superstructure is clearly observed for the odd stacks (bottom panels) and for the thicker even stacks (top right panel). All results presented in this figure are obtained using 2D PBC boundary conditions optimizations. For clarity of the presentation, the simulation box (marked by a black rectangle in each panel) is multiplied in the lateral directions. The color scale denotes the vertical height of the atoms in the top layer with respect to its center of mass.

6 layers the flamingo pattern is found to be the most stable one (see Secs. 2.3 and 4 of the SM [40] for thicker heterostructures results). This is further supported by our 3D PBC calculations that exhibit the same preference for the flamingolike superstructure [see Fig. 1(e)]. Notably, for the 12-layered model stack, where both 2D and 3D PBC results are presented, the superstructure obtained by the 3D PBC calculations (full symbols) is somewhat less corrugated than that obtained via 2D PBC calculations (open symbols) indicating that the bulk limit is not yet reached at this thickness. This is a physical effect that is expected to be found also in experiments.

The predicted parity dependence of the vertical deformation superstructure opens a route to design the mechanical properties of layered materials heterostructures. To demonstrate this, we evaluate the Young's modulus and Poisson's ratio for graphene/h-BN alternating heterostructures of varying thickness (the corresponding simulation protocol is presented in Sec. 1.4 of the SM [40] and the raw simulation data can be found in Sec. 5 of the SM [40]). The results are summarized in Fig. 3.

From Figs. 3(a) and 3(b) it is evident that both Young's modulus and Poisson's ratio exhibit strong parity dependence (up to a factor of 2 and 50, respectively) when the number of layers is smaller than 7. The parity dependence disappears for thicker stacks, consistent with the deformation pattern behavior discussed above. Increasing the temperature from 5 to 300 K has minor effect on the parity dependence of the elastic constants [see Figs. 3(c) and 3(d) and Secs. 5–6 of the SM [40]]. The value of the Young's modulus for the alternating graphene/h-BN heterostructure (∼240 GPa) is much lower than that of monolayer graphene (∼1000 GPa) [49] and h-BN (∼865 GPa) [50]. We attribute this to the highly corrugated nature of the heterostructures that can flatten upon loading while reducing in-plane covalent bond elongation stress (see Sec. 7 in the SM [40]). For thin stacks ($N < 7$) at 5 K, the Poisson's ratio [Fig. 3(b)] of the even-numbered systems is positive and in the range of 0.1–0.3, whereas for odd numbered systems it is minute (∼|0.04|) and changes sign when the direction of the applied strain is switched. When the number of layers exceeds seven, the parity dependence of Poisson's ratio disappears and its value ranges from −0.046 to −0.0045 and from 0.058 to

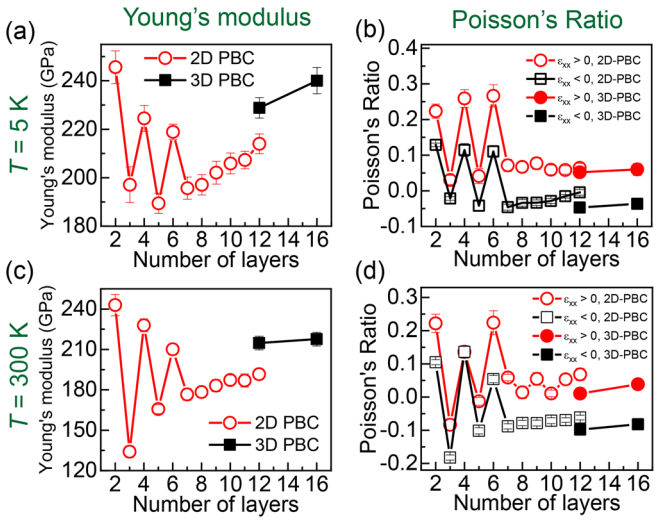

FIG. 3. Parity dependence of the mechanical properties of alternating graphene/h-BN heterostructures. (a),(c) Young's modulus and (b),(d) Poisson's ratio as functions of the number of layers evaluated at a temperature of $T = 5$ K (upper panels) and $T = 300$ K (lower panels), respectively. Open symbols (full symbols) represent calculations obtained using 2D (3D) PBC with different supercell thicknesses. In panels (b) and (d), results for both stretching (red circles) and compression (black squares) strains are presented to emphasize the dependence of Poisson's ratio on the loading direction. The error bars represent the standard deviation obtained in the calculation of the corresponding coefficients (see Figs. S10–S13 in the SM [40] for further details).

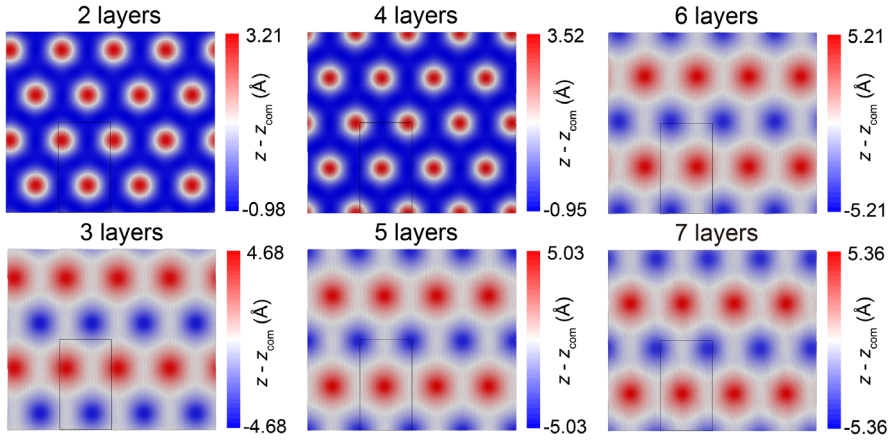

FIG. 4. The out-of-plane deformation pattern of alternating twisted graphene heterostructures. Each even numbered layer is rotated by 1.12° with respect to its adjacent odd numbered layers. To show the deformation pattern clearly, the simulation box (marked by a black rectangle in each panel) is multiplied in the lateral directions. The color scales denote the perpendicular height of the top layer atoms with respect to the center of mass of the layer.

0.077 for compression and stretching deformations, respectively (these small values should be considered qualitatively in light of the approximate nature of our classical molecular dynamics computational approach). The values of Poisson's ratio calculated at room temperature are very similar to those obtained at 5 K [see Fig. 3(d) and Secs. 5 and 6 in the SM [40]]. We note that small Poisson's ratio materials have recently attracted much attention due to their potential utilization in many advanced applications [51–54].

The discovered parity dependence of the vertical deformation patterns is attributed to the intricate interplay between the large-scale moiré superlattices formed at each interface in the heterostructures. In fact, while all odd-numbered stacks presented here possess an excess *h*-BN layer, similar results were obtained for odd heterostructures with an excess graphene layer (see Sec. 4.2 of the SM [40] for further details). This suggests that the phenomenon is not limited to the case of graphene/*h*-BN heterostructures but should be observed for many alternating vdW layered stacks of closely matched lattice vectors, where large moiré superlattices are formed between adjacent layers. Notably, this can also be achieved in homogeneous alternating layered stacks, where adjacent layers assume a misaligned configuration. To demonstrate this, we constructed multilayer alternating twisted homogeneous graphene and *h*-BN stack models, where the even numbered layers are rotated by 1.12° with respect to their odd numbered counterparts. As shown in Fig. 4, the out-of-plane deformation pattern of the twisted graphitic system exhibits clear parity dependence on the number of stacked layers with large variations of its out-of-plane corrugation. Similar results for homogeneous twisted alternating *h*-BN stacks are presented in Sec. 8 of the SM [40]. Since several recent studies already demonstrated delicate control over the misfit angle of 2D material interfaces [17,55], we expect that the fabrication of such structures will become feasible in the near future.

The fact that parity dependence appears in both homogeneous and heterogenous alternating structures and that the flamingo patterns are found in heterostructures with either graphene or *h*-BN excess layers, demonstrates the general nature of the predicted phenomenon. Together with the nearly vanishing Poisson's ratio exhibited by the flamingo-shaped superstructure materials, our findings therefore suggest the possibility to construct a new type of metamaterials with tunable mechanical properties.

W. O. acknowledges the financial support from the National Natural Science Foundation of China (No. 11890673 and No. 11890674) and the National Supercomputer Center in Tianjin for performing part of the simulations on the TianHe-1(A) cluster. M. U. acknowledges the financial support of the Israel Science Foundation, Grant No. 1141/18 and the ISF-NSFC joint Grant No. 3191/19. O. H. is grateful for the generous financial support of the Israel Science Foundation under Grant No. 1586/17, Tel Aviv University Center for Nanoscience and Nanotechnology, and the Naomi Foundation for generous financial support via the Kadar Award. O. H. and M. U. directed the project. W. O. wrote the code and conducted the simulations. All authors conceived the original idea, designed the simulations, analyzed the results, and wrote the manuscript. The authors declare no conflict of interest.

*odedhod@tauex.tau.ac.il

[1] A. Geim and I. Grigorieva, Van der Waals heterostructures, Nature (London) **499**, 419 (2013).

[2] I. Leven, D. Krepel, O. Shemesh, and O. Hod, Robust superlubricity in graphene/*h*-BN heterojunctions, J. Phys. Chem. Lett. **4**, 115 (2013).

[3] K. S. Novoselov, A. Mishchenko, A. Carvalho, and A. H. Castro Neto, 2D materials and van der Waals heterostructures, Science **353**, aac9439 (2016).

[4] O. Hod, E. Meyer, Q. Zheng, and M. Urbakh, Structural superlubricity and ultralow friction across the length scales, Nature (London) **563**, 485 (2018).

[5] S. Zhang, T. Ma, A. Erdemir, and Q. Li, Tribology of two-dimensional materials: From mechanisms to modulating strategies, Mater. Today **26**, 67 (2019).

[6] Y. Gong *et al.*, Vertical and in-plane heterostructures from WS_2/MoS_2 monolayers, Nat. Mater. **13**, 1135 (2014).

[7] S. Gupta, A. Kutana, and B. I. Yakobson, Heterobilayers of 2D materials as a platform for excitonic superfluidity, Nat. Commun. **11**, 2989 (2020).

[8] J. Wang, F. Ma, and M. Sun, Graphene, hexagonal boron nitride, and their heterostructures: Properties and applications, RSC Adv. **7**, 16801 (2017).

[9] L. Britnell *et al.*, Field-effect tunneling transistor based on vertical graphene heterostructures, Science **335**, 947 (2012).

[10] C. R. Dean *et al.*, Boron nitride substrates for high-quality graphene electronics, Nat. Nanotechnol. **5**, 722 (2010).

[11] C.-C. Chen, Z. Li, L. Shi, and S. B. Cronin, Thermoelectric transport across graphene/hexagonal boron nitride/graphene heterostructures, Nano Res. **8**, 666 (2015).

[12] X. Li, S. Lin, X. Lin, Z. Xu, P. Wang, S. Zhang, H. Zhong, W. Xu, Z. Wu, and W. Fang, Graphene/*h*-BN/GaAs sandwich diode as solar cell and photodetector, Opt. Express **24**, 134 (2016).

[13] F. Withers *et al.*, Light-emitting diodes by band-structure engineering in van der Waals heterostructures, Nat. Mater. **14**, 301 (2015).

[14] F. Withers *et al.*, WSe_2 light-emitting tunneling transistors with enhanced brightness at room temperature, Nano Lett. **15**, 8223 (2015).

[15] A. Mishchenko *et al.*, Twist-controlled resonant tunnelling in graphene/boron nitride/graphene heterostructures, Nat. Nanotechnol. **9**, 808 (2014).

[16] J. R. Wallbank *et al.*, Tuning the valley and chiral quantum state of Dirac electrons in van der Waals heterostructures, Science **353**, 575 (2016).

[17] E. Koren, I. Leven, E. Lörtscher, A. Knoll, O. Hod, and U. Duerig, Coherent commensurate electronic states at the interface between misoriented graphene layers, Nat. Nanotechnol. **11**, 752 (2016).

[18] Y. Cao, V. Fatemi, S. Fang, K. Watanabe, T. Taniguchi, E. Kaxiras, and P. Jarillo-Herrero, Unconventional superconductivity in magic-angle graphene superlattices, Nature (London) **556**, 43 (2018).

[19] Z. Wang *et al.*, Composite super-moiré lattices in double-aligned graphene heterostructures, Sci. Adv. **5**, eaay8897 (2019).

[20] C. R. Dean *et al.*, Hofstadter's butterfly and the fractal quantum Hall effect in moiré superlattices, Nature (London) **497**, 598 (2013).

[21] B. Hunt *et al.*, Massive Dirac fermions and Hofstadter butterfly in a van der Waals heterostructure, Science **340**, 1427 (2013).

[22] D. Mandelli, W. Ouyang, M. Urbakh, and O. Hod, The princess and the manoscale pea: Long-range penetration of surface distortions into layered materials stacks, ACS Nano **13**, 7603 (2019).

[23] Y. Song, D. Mandelli, O. Hod, M. Urbakh, M. Ma, and Q. Zheng, Robust microscale superlubricity in graphite/hexagonal boron nitride layered heterojunctions, Nat. Mater. **17**, 894 (2018).

[24] W. Ouyang, D. Mandelli, M. Urbakh, and O. Hod, Nanoserpents: Graphene nanoribbon motion on two-dimensional hexagonal materials, Nano Lett. **18**, 6009 (2018).

[25] D. Mandelli, W. Ouyang, O. Hod, and M. Urbakh, Negative Friction Coefficients in Superlubric Graphite-Hexagonal Boron Nitride Heterojunctions, Phys. Rev. Lett. **122**, 076102 (2019).

[26] C. R. Woods *et al.*, Commensurate-incommensurate transition in graphene on hexagonal boron nitride, Nat. Phys. **10**, 451 (2014).

[27] G. J. Slotman, M. M. van Wijk, P. L. Zhao, A. Fasolino, M. I. Katsnelson, and S. Yuan, Effect of Structural Relaxation on the Electronic Structure of Graphene on Hexagonal Boron Nitride, Phys. Rev. Lett. **115**, 186801 (2015).

[28] E. M. Alexeev *et al.*, Resonantly hybridized excitons in moiré superlattices in van der Waals heterostructures, Nature (London) **567**, 81 (2019).

[29] M. Anđelković, S. P. Milovanović, L. Covaci, and F. M. Peeters, Double moiré with a twist: Supermoiré in encapsulated graphene, Nano Lett. **20**, 979 (2020).

[30] H. Goto, E. Uesugi, R. Eguchi, and Y. Kubozono, Parity effects in few-layer graphene, Nano Lett. **13**, 5153 (2013).

[31] M. Koshino and E. McCann, Parity and valley degeneracy in multilayer graphene, Phys. Rev. B **81**, 115315 (2010).

[32] G. N. Greaves, A. L. Greer, R. S. Lakes, and T. Rouxel, Poisson's ratio and modern materials, Nat. Mater. **10**, 823 (2011).

[33] R. S. Lakes, Negative-Poisson's-ratio materials: Auxetic solids, Annu. Rev. Mater. Res. **47**, 63 (2017).

[34] Y. Wen, E. Gao, Z. Hu, T. Xu, H. Lu, Z. Xu, and C. Li, Chemically modified graphene films with tunable negative Poisson's ratios, Nat. Commun. **10**, 2446 (2019).

[35] D. W. Brenner, O. A. Shenderova, J. A. Harrison, S. J. Stuart, B. Ni, and S. B. Sinnott, A second-generation reactive empirical bond order (REBO) potential energy expression for hydrocarbons, J. Phys. Condens. Matter **14**, 783 (2002).

[36] A. Kınacı, J. B. Haskins, C. Sevik, and T. Cagin, Thermal conductivity of BN-C nanostructures, Phys. Rev. B **86**, 115410 (2012).

[37] I. Leven, T. Maaravi, I. Azuri, L. Kronik, and O. Hod, Interlayer potential for graphene/*h*-BN heterostructures, J. Chem. Theory Comput. **12**, 2896 (2016).

[38] T. Maaravi, I. Leven, I. Azuri, L. Kronik, and O. Hod, Interlayer potential for homogeneous graphene and hexagonal boron nitride systems: Reparametrization for many-body dispersion effects, J. Phys. Chem. C **121**, 22826 (2017).

[39] W. Ouyang, I. Azuri, D. Mandelli, A. Tkatchenko, L. Kronik, M. Urbakh, and O. Hod, Mechanical and tribological properties of layered materials under high pressure: Assessing the importance of many-body dispersion effects, J. Chem. Theory Comput. **16**, 666 (2020).

[40] See Supplemental Material at http://link.aps.org/supplemental/10.1103/PhysRevLett.126.216101 for methodology, comparison of minimization protocols, convergence tests, additional optimized heterostructures, raw data for calculating Young's modulus and Poisson's ratio, thermal expansion of bulk graphene/*h*-BN heterostructures, effect of strain on the out-of-plane corrugation of graphene/*h*-BN heterostructures, and parity-dependent superlattices in alternating twisted *h*-BN heterostructures. The Supplemental Material includes Refs. [41–47].

[41] S. Alexander, Visualization and analysis of atomistic simulation data with OVITO—The Open Visualization Tool, Model. Simul. Mater. Sci. Eng. **18**, 015012 (2010).

[42] S. Plimpton, Fast parallel algorithms for short-range molecular dynamics, J. Comput. Phys. **117**, 1 (1995).

[43] W. Shinoda, M. Shiga, and M. Mikami, Rapid estimation of elastic constants by molecular dynamics simulation under constant stress, Phys. Rev. B **69**, 134103 (2004).

[44] E. Bitzek, P. Koskinen, F. Gähler, M. Moseler, and P. Gumbsch, Structural Relaxation Made Simple, Phys. Rev. Lett. **97**, 170201 (2006).

[45] G. Henkelman and H. Jónsson, Improved tangent estimate in the nudged elastic band method for finding minimum energy paths and saddle points, J. Chem. Phys. **113**, 9978 (2000).

[46] G. Henkelman, B. P. Uberuaga, and H. Jónsson, A climbing image nudged elastic band method for finding saddle points and minimum energy paths, J. Chem. Phys. **113**, 9901 (2000).

[47] W. Ouyang, H. Qin, M. Urbakh, and O. Hod, Controllable thermal conductivity in twisted homogeneous interfaces of graphene and hexagonal boron nitride, Nano Lett. **20**, 7513 (2020).

[48] M. M. van Wijk, A. Schuring, M. I. Katsnelson, and A. Fasolino, Moiré Patterns as a Probe of Interplanar Interactions for Graphene on *h*-BN, Phys. Rev. Lett. **113**, 135504 (2014).

[49] C. Lee, X. Wei, J. W. Kysar, and J. Hone, Measurement of the elastic properties and intrinsic strength of monolayer graphene, Science **321**, 385 (2008).

[50] A. Falin *et al.*, Mechanical properties of atomically thin boron nitride and the role of interlayer interactions, Nat. Commun. **8**, 15815 (2017).

[51] Y. Wu *et al.*, Three-dimensionally bonded spongy graphene material with super compressive elasticity and near-zero Poisson's ratio, Nat. Commun. **6**, 6141 (2015).

[52] X. Xu, Q. Zhang, Y. Yu, W. Chen, H. Hu, and H. Li, Naturally dried graphene aerogels with superelasticity and tunable Poisson's ratio, Adv. Mater. **28**, 9223 (2016).

[53] J. N. Grima and D. Attard, Molecular networks with a near zero Poisson's ratio, Phys. Status Solidi B **248**, 111 (2011).

[54] X. Li, C. Huang, S. Hu, B. Deng, Z. Chen, W. Han, and L. Chen, Negative and near-zero Poisson's ratios in 2D graphene/MoS_2 and graphene/*h*-BN heterostructures, J. Mater. Chem. C **8**, 4021 (2020).

[55] Z. Yu, A. Song, L. Sun, Y. Li, L. Gao, H. Peng, T. Ma, Z. Liu, and J. Luo, Understanding interlayer contact conductance in twisted bilayer graphene, Small **16**, 1902844 (2020).